Supporting Information

Constructing thiophene-decorated organic molecular sieves as efficient photocatalysts for removing chromium(VI)

Jingjing Ge,[a,b] Lingkang Meng,[b] Xin Xu,[b] Xin He,[b] Jiaxin Chu,[b] Wan-Kai An*[b], Lixia Xie,[b] Xianfu Zheng,[b] and Yunlai Ren*[b]

[a]*College of Chemistry, Zhengzhou University, Zhengzhou, Henan 450001, P.R. China.*
[b]*College of Science, Henan Agricultural University, Zhengzhou, Henan 450002, China. E-mail: anwk@henau.edu.cn; renyunlai@126.com.*

List of Contents

I. General Information

Materials. 1,3,5-tris[(*p*-boronicacid)phenyl]benzene (TBPB)[1], 2,5-dibromothieno[3,2-b]thiophene (TBTP-2Br)[2-3] and were prepared according to the literature procedures. Other reagents can be purchased from commercial suppliers (Energy Chemical Reagent Co. Ltd and Adamas Reagent Co. Ltd) used without further purification, unless otherwise noted. Pd-mediated coupling reactions were carried out under N_2 by using Schlenk line techniques. The deionized water was used during the synthesis of porous materials.

Methods. Liquid NMR spectra (^1H and ^{13}C) were recorded on a Bruker Avance III 400 MHz NMR spectrometer ($CDCl_3$ or d_6-acetone as solvent). The chemical shifts δ and coupling constants J are given in ppm and Hz, respectively. Powder X-ray diffraction (PXRD) data were collected with a TD-3500 X-ray diffractometer operated at 30 kV and 20 mA with Cu Kα radiation at a scan rate of 15°/min. Nitrogen adsorption and desorption isotherms were measured at 77 K using a Quantachrome NovaWin 2200e system. The samples were outgassed at 120 °C for 8 h before analysis. Surface areas were calculated based on the adsorption data via the Brunauer-Emmett-Teller (BET) and Langmuir methods, respectively. The pore-size-distribution (PSD) curves were obtained from the adsorption branches using non-local density functional theory (NLDFT) method. The pore volume was calculated from the amount of N_2 gas adsorbed at $P/P_0 = 0.99$ based on the *t*-plot analysis.

The FT-IR spectra were acquired using the Nicolet IS-20 instrument. Thermogravimetric analysis (TGA) measurements were used to study the thermal stability of the porous organic polymers. The tests were carried out on a SDT Q600 (V20.9 Build 20) instrument from 25 to 800 °C under a N_2 atmosphere with a heating rate of 10 °C/min. Elemental analysis was performed on a Vario EL cube instrument. Scanning electron microscope (SEM) tests were applied to analysis the surface morphologies and microstructures of the obtained materials with Thermo Fisher F200X at a voltage of 15 kV. The samples used for SEM analysis were dispersed in ethanol, and then dipped and dried on a silicon wafer. To detect the elemental compositions within the porous networks, part regions in SEM analytical samples were selected to collect the Energy-dispersive X-ray spectroscopic (EDS) data at a voltage of 15 kV. The palladium contents of the polymeric samples were determined by inductively coupled plasma (ICP) analysis with a TJA IRIS Advantage ER/S instrument.

UV-Vis diffuse reflectance analysis (DRS) for TP-OMSs was recorded on a Persee TU-1901 model spectrometer equipped with integration sphere. The bandgaps were estimated from the UV-Vis diffuse reflectance spectra through Tauc plots. Electrochemical experiments were conducted on CHI660E Electrochemical Workstation by using a three-electrode electrochemical cell (ITO working electrode, a saturated calomel electrode (SCE) as reference electrode, platinum wire as counter electrode, 0.2 M Na_2SO_4 aq. as electrolyte). According to the experimental requirements, the electrode potential *vs.* SCE was converted and expressed as the relative electrode potential to the normal hydrogen electrode (NHE) using the following equation: $E_{\mathrm{NHE}} = E_{\mathrm{SCE}} + E_{SCE}^{\theta}$ ($E_{SCE}^{\theta} = +0.2415$ V). The photocurrent measurements were performed in by illumination using 40 W LEDs at intervals of 15 seconds. The working electrodes for photocurrent and electrochemical impedance spectroscopy (EIS) measurements were prepared by pasting slurry of TZ-OMS (5.0 mg) in 5% Nafion/EtOH (50 μL/50 μL) onto the ITO conductive glass, dried under air, and then immersed in Na_2SO_4 aqueous solution (0.2 M). Electron paramagnetic resonance (EPR) spectra were conducted on Bruker A300. The X-ray photoelectron spectroscopy (XPS) analysis was performed on Thermo Fisher ESCAlab 250Xi.

II. Synthetic Procedures

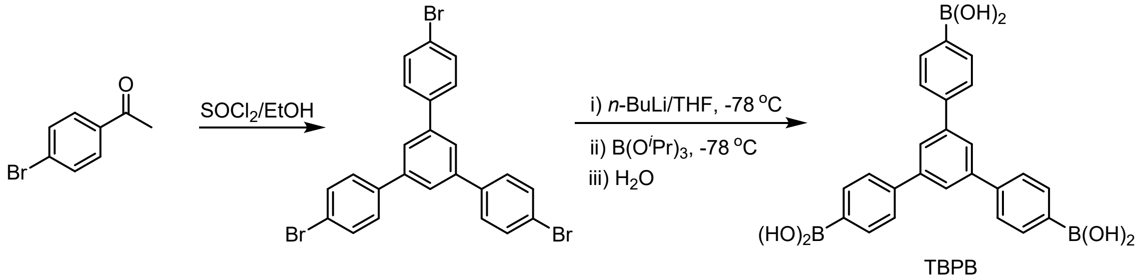

Scheme S1. Synthesis of 1,3,5-tris[(p-boronicacid)phenyl]benzene.

Synthesis of 1,3,5-tris[(p-boronicacid)phenyl]benzene (TBPB)[1]

Under 0 °C, a 100 mL two-neck flask with reflux condenser and exhaust treatment device was charged with *p*-bromoacetophenone (0.1 mol, 20 g) in EtOH (30 mL). Under vigorous stirring, a solution of 20 mL $SOCl_2$ (32.8 g, 0.276 mol) was added dropwise *via* injection pump over a period of 1 hour. The reaction mixture was allowed to reach ambient temperature and stirred overnight at 60 °C. Subsequently, the resulting suspension was cooled in an ice bath and carefully treated with 0.2 L water while stirring to induce HCl evolution. The resulting precipitate was collected, washed with hot ethanol until the filtrate became colorless, and finally dried under reduced pressure to yield pale yellow solid of 1,3,5-tris(*p*-bromophenyl)benzene[4] (15.0 g, 83%). ^{1}H NMR (400 MHz, $CDCl_3$): δ = 7.69 (s, 3H), 7.61 (d, J = 4.4 Hz, 6 H), 7.53 (d, J = 4.4 Hz, 6 H) ppm; ^{13}C NMR (100 MHz, $CDCl_3$): δ = 141.5, 139.6, 132.1, 128.9, 125.0, 122.1 ppm.

The solution of 1,3,5-tris(*p*-bromophenyl)benzene[1] (1.36 g, 2.5 mmol) was vigorously stirred in anhydrous THF (50 mL), while gradually adding a solution of *n*-BuLi in hexanes (1.6 M, 7.8 mL, 12.5 mmol) at -78 ° C. Following one hour of stirring at -78 ° C, B(O^{i}Pr)$_3$ (3.2 mL, 13.7 mmol) was slowly added into the reaction mixture and stirred for another hour at -78 ° C before being warmed to room temperature and then stirred for overnight. The reaction was terminated by adding 25 mL saturated aqueous NH_4Cl solution. The mixtures were extracted with CH_2Cl_2 (three times) to obtain the combined organic layers. The organic layers were concentrated and yielded a white solid, which was then recrystallized from methanol/hexanes to form a white TBPB. ^{1}H NMR (400 MHz, acetone-d_6): δ = 8.03 (d, J = 3.4 Hz, 6 H), 7.98 (s, 3H), 7.87 (d, J = 4.0 Hz, 6 H), 7.26-7.24 (br, 6H) ppm; ^{13}C NMR (100 MHz, acetone-d_6): δ = 142.6, 142.3, 134.8, 126.4, 124.9 ppm.

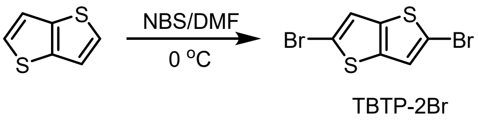

Scheme S2. Synthesis of TBTP-2Br.

Synthesis of monomer TBTP-2Br[2-3]. N-Bromosuccinimide (3.58 g, 20 mmol) was added slowly into a stirred solution of thieno[3,2-b] thiophene (1.40 g, 10 mmol) in N,N-dimethylformamide (DMF, 20 mL) under 0 °C. The system was stirred for 3 h at room temperature and then water was added to quench the reaction. The mixture was extracted with diethyl ether, and the collected organic phase was dried over anhydrous Na_2SO_4. After removing the excess solvent under reduced pressure, the crude product was purified by flash silica gel column chromatography using petroleum ether as the eluent to give product TBTP-2Br as white solid (2.5 g, 84% yield). ^{1}H NMR (400 MHz, $CDCl_3$): δ = 7.17 (s, 2H) ppm; ^{13}C NMR (100 MHz, $CDCl_3$): δ = 138.28, 121.77, 113.62 ppm.

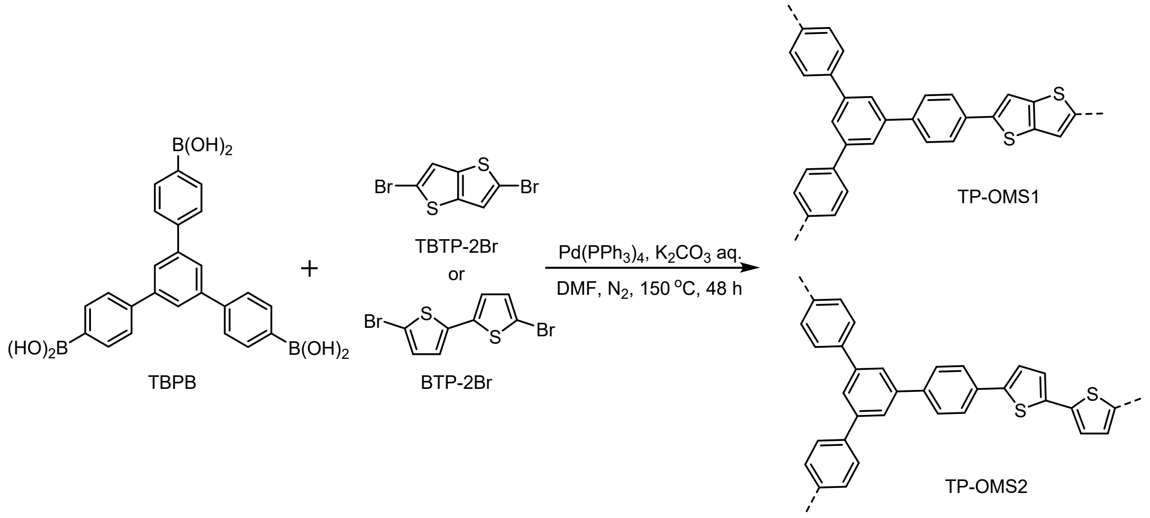

Scheme S3. Synthesis of TP-OMS1 and TP-OMS2.

Synthesis of TP-OMS1 and TP-OMS2. TP-OMS1 and TP-OMS2 were prepared *via* Suzuki-Miyaura coupling reaction. A two-necked flask was charged with TBPB (87.6 mg, 0.2 mmol), dibromo-substituted thiophene derivatives TBTP-2Br (89.4 mg, 0.3 mmol) or BTP-2Br (97.2 mg, 0.3 mmol), $Pd(PPh_3)_4$ (9.2 mg, 0.008 mmol). And then DMF (8 mL) and 2 M K_2CO_3 aqueous solution (1.6 mL) were added into the flask. The reaction mixture was stirred and bubbled by N_2 ball for 0.5 hours at room temperature. Then, the system was stirred under 150 °C and N_2 atmosphere for 2 days. After cooling to ambient temperature, the precipitate was filtrated and washed in turn with water, DMF, EtOH. The resulting solid was further purified by the Soxhlet extraction for 12 h with THF and

MeOH as solvent, respectively. After drying at 80 °C for 12 h, the conjugated microporous polymers were obtained as yellow-green (TP-OMS1, 93% yield) or yellow powder (TP-OMS2, 86% yield). As identified by Inductively Coupled Plasma Mass Spectrometry (ICP-MS) analysis, the residual Pd contents within TP-OMS1 was 0.148% for TP-OMS1.

III. Characterization of TP-OMSs

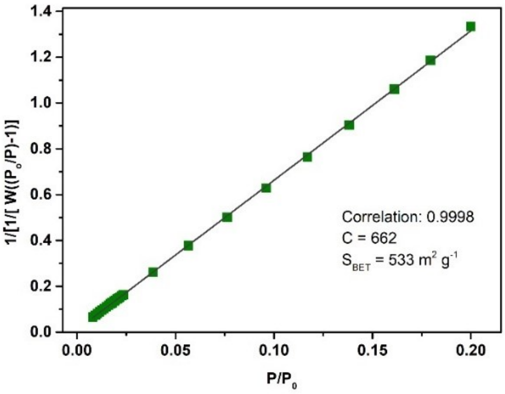

Figure S1. BET surface area plot for TP-OMS1.

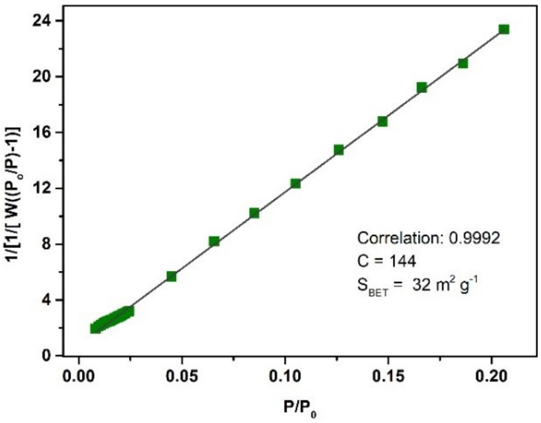

Figure S2. BET surface area plot for TP-OMS2.

Table S1. Summary of S_{BET} for TP-OMS2 prepared in different conditions.[a]

Solvent	T (°C)	Yield (%)	S_{BET} (m^2 g^{-1})
DMF	150	86	32
THF	80	76	3
DMAc	150	51	43
Toluene	100	33	21

[a] General conditions: TBPB (0.1 mmol), BTP-2Br (0.15 mmol), Pd(PPh$_3$)$_4$ (4 mol%), solvent (4 mL), 2 M K$_2$CO$_3$ (0.8 mL), N$_2$, 48 h. [b] TBPB (0.2 mmol), BTP-2Br (0.3 mmol), Pd(PPh$_3$)$_4$ (4 mol%), solvent (8 mL), 2 M K$_2$CO$_3$ (1.6 mL). S_{BET}: BET surface area.

Discussions about the adsorption behaviours of TP-OMSs:

The inherent structures of materials determine their adsorption behaviors. TP-OMSs are synthesized *via* coupling reaction and have low reversibility. The thermodynamic factors could cause molecular structural distortions during the formation and precipitation of the OMSs. Consequently, TP-OMSs do not exhibit conventional 2D topological features but rather form 3D amorphous frameworks.[5] This results in complex pore channels within the materials, potentially featuring *"ink bottle" pores, tubular pores, and interstitial pores* because of spherical particles packing. The pore size distribution is irregular, and the precise determination for pore shapes is not easy.

We speculate that the hysteresis loss of TP-OMS1 is analogous to that of type H2 (Figure 2a). Herein, *this hysteresis can be attributed to the akinetic effect, or the 'dual mode sorption', i.e., the swelling of the polymer matrix by nitrogen after all initial micropores have been filled.*[6] Notably, the adsorption-desorption isotherm of TP-OMS1 exhibits an open state. The swelling properties of the porous polymers caused deformation of the pore channels during gas adsorption-desorption. This phenomenon is also observed in other porous organic polymers.[6-8]

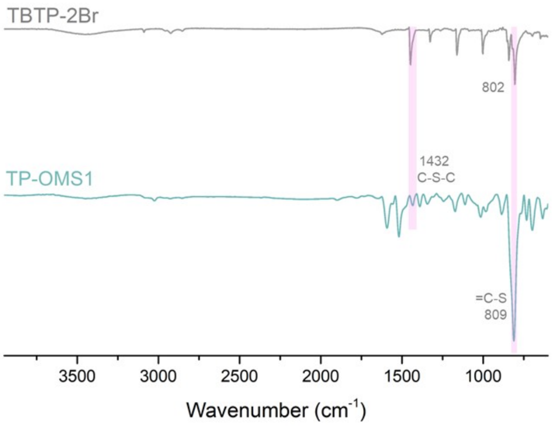

Figure S3. FT-IR spectra of TBTP-2Br and TP-OMS1.

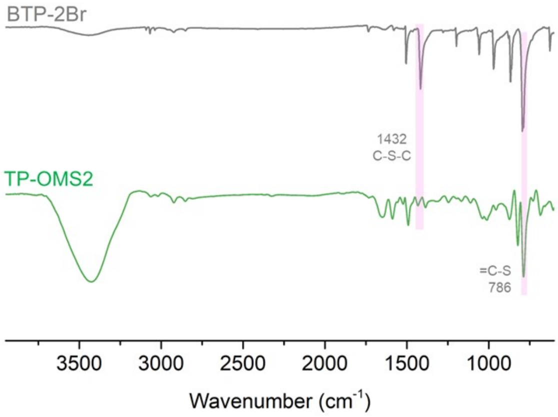

Figure S4. FT-IR spectra of BTP-2Br and TP-OMS2.

The FT-IR spectra (Figure S1 and S2) of TP-OMSs showed peaks at 809 $cm^{-1}$and 786 cm^{-1}, which demonstrated the presence of =C-S bonds that come from thieno[3,2-b]thiophene and 2,2'-bithiophene units, respectively.[2, 9-11] Meanwhile, the two OMSs showed stretching vibration signals (1432 cm^{-1}) for C-S-C that derived from thiophenes.[12] Theses peaks proved that 2,2'-bithiophene and thieno[3,2-b]thiophene units have been incorporated into the frameworks of TP-OMSs.

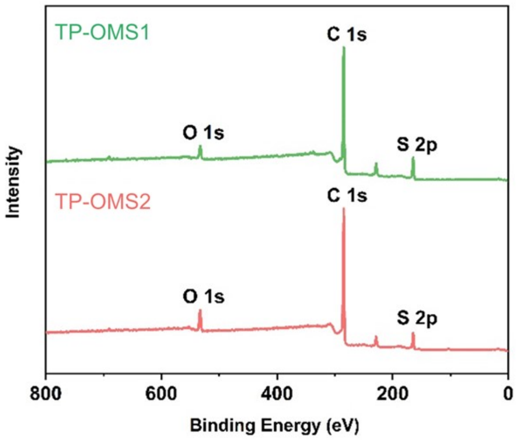

Figure S5. The survey XPS of TP-OMSs.

The XPS spectra confirmed the presence of carbon and sulfur in the material, while the origin of oxygen could be attributed to potential external contamination or residual oxygen-containing precursors or inorganic salts.

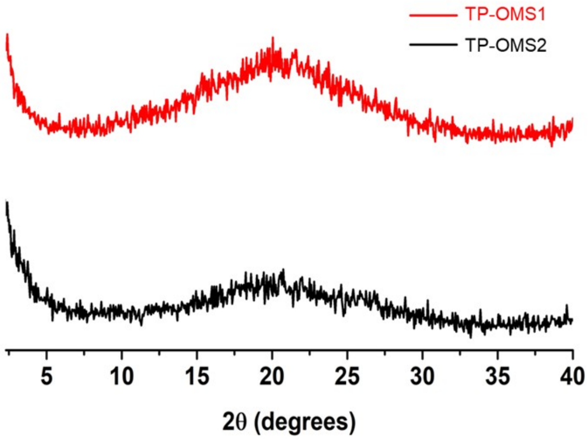

Figure S6. Powder X-ray diffraction of TP-OMSs. These results proved that both TP-OMS1 and TP-OMS2 were amorphous materials.

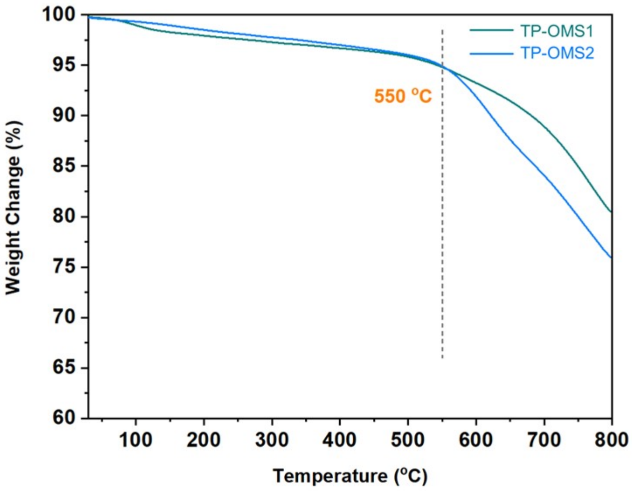

Figure S7. TGA curves of TP-OMS1 (dark cyan) and TP-OMS2 (light blue). The two OMSs were enough stable up to about 550 °C and with finally leftover weight of 82%/76% under N_2 atmosphere.

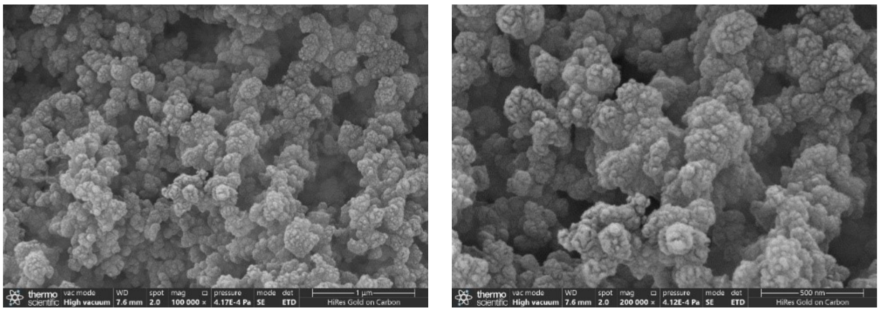

Figure S8. SEM images of TP-OMS1

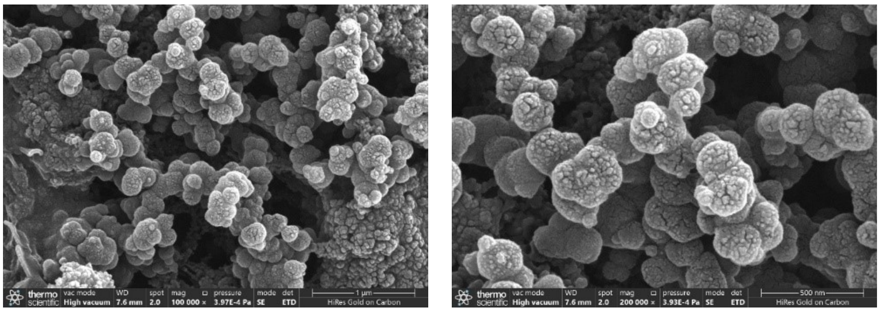

Figure S9. SEM images of TP-OMS2

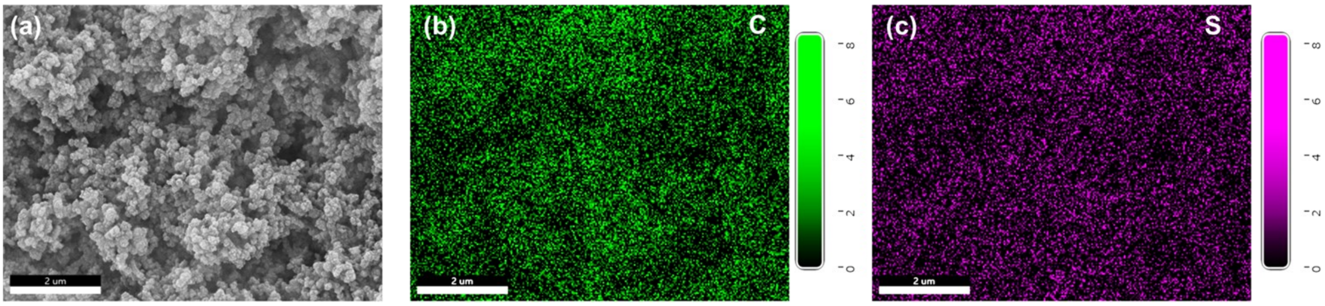

Figure S10. EDS mapping images of C and S for TP-OMS1.

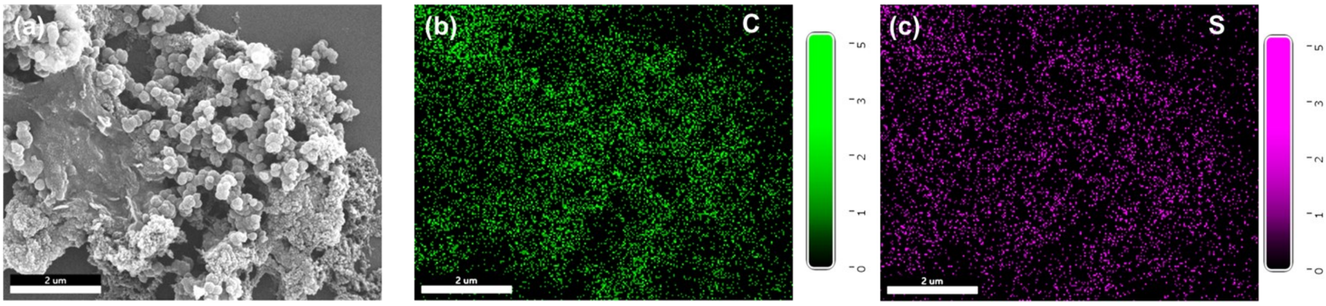

Figure S11. EDS mapping images of C and S for TP-OMS2.

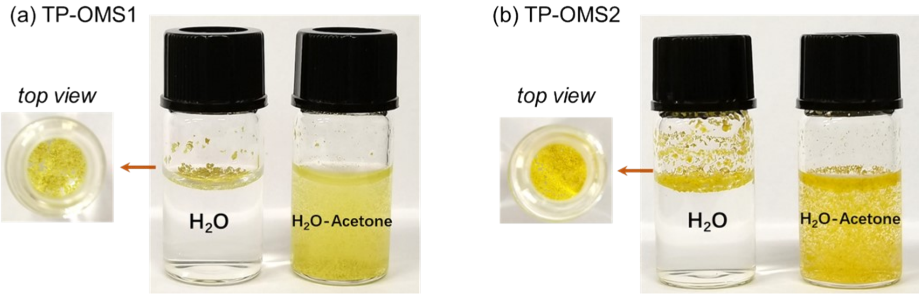

Figure S12. Dispersion in H_2O or H_2O/acetone (25/1) of TP-OMSs.

HOMO/LUMO	TP-OMS$_{1A}^{\dagger}$	TP-OMS$_{1B}^{\dagger}$	TP-OMS$_{1C}^{\dagger}$
LUMO	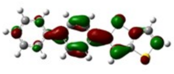 -1.69 eV	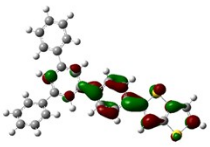 -1.72 eV	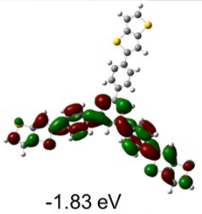 -1.83 eV
HOMO	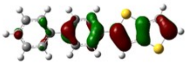 -5.65 eV	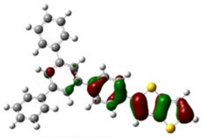 -5.67 eV	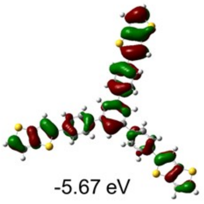 -5.67 eV
HOMO-LUMO gap	3.96 eV	3.95 eV	3.84 eV

Figure S13. B3LYP/6-311G (d, p) calculated HOMO and LUMO figures for the selected neutral catalytic unit (TP-OMS1†) in TP-OMS1. The experiments were conducted with Gaussian 09 software.

HOMO/LUMO	TP-OMS$_{2A}$†	TP-OMS$_{2B}$†	TP-OMS$_{2C}$†
LUMO	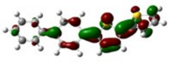 -1.82 eV	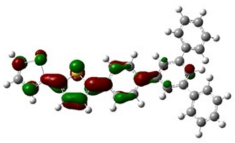 -1.85 eV	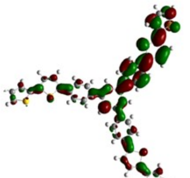 -1.95 eV
HOMO	 -5.49 eV	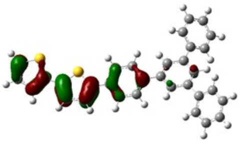 -5.50 eV	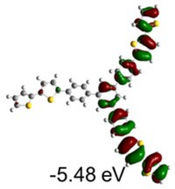 -5.48 eV
HOMO-LUMO gap	3.67 eV	3.65 eV	3.53 eV

Figure S14. B3LYP/6-311G (d, p) calculated HOMO and LUMO figures for the selected neutral catalytic unit (TP-OMS1†) in TP-OMS2. The experiments were conducted with Gaussian 09 software.

IV. Photoreduction of Cr(VI)

Standard procedures: TP-OMSs (5 mg) and of Cr(VI) aqueous solution (10 mg L^{-1}, 5 mL) were mixed with acetone (0.2 mL) to enhance the dispersion effect in water. The mixture was stirred under dark and sealed conditions for 2 hours to achieve adsorption-desorption equilibrium (the time was recorded as -2.0 h). The stirred mixture was then exposed to 6 W blue light irradiation under an air atmosphere. Liquid samples were timely collected from the reaction solution at different time intervals (*e.g.*, 0.5 h). The collected solutions were treated with 0.2 M H_2SO_4 solution (4.5 mL) and 0.20% DPC solution (0.1 mL). Then, the absorbance was measured using a UV-visible spectrophotometer.

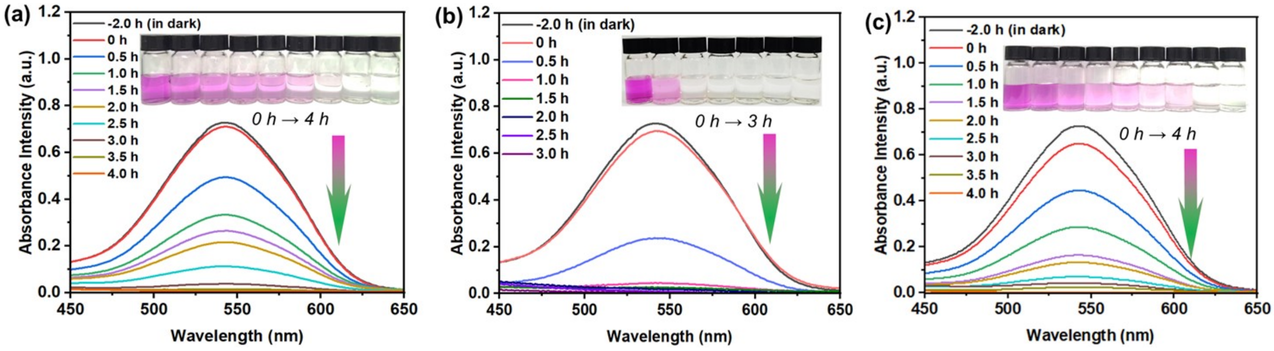

Figure S15. Time-dependent absorbance and color changes of Cr(VI) derived by different dosage of TP-OMSs: (a) 2.5 mg, (b) 5.0 mg, (c) 7.5 mg. *The collected Cr(VI) solutions were treated with H_2SO_4 and DPC solution to form colored solutions for UV-visible spectra measurement.*

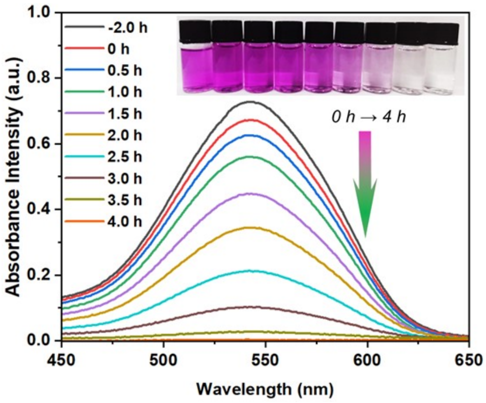

Figure S16. Time-dependent absorbance and color changes of Cr(VI) (C_0 = 100 mg L^{-1}) derived by 5 mg of TP-OMS1. *Herein, the collected Cr(VI) solutions were first diluted with water in a ratio of 10:1, and then treated with H_2SO_4 and DPC to form colored solutions for UV-visible spectra measurement.*

V. Recyclability Tests of TP-OMS1

General procedures: TP-OMSs (5 mg) and 5 mL of Cr(VI) aqueous solution (10 mg L^{-1}) were mixed with 0.2 mL of acetone (as a dispersant). The mixture was stirred under dark and sealed conditions for 2 hours to achieve adsorption-desorption equilibrium (the time was recorded as -2.0 h). The stirred mixture was then exposed to 6 W blue light irradiation under an air atmosphere. The Cr(VI) solution was measured using the aforementioned established methods: The liquid supernatants were timely collected from the reaction solution after appropriate time (*e.g.*, 2.5 h), then were first treated with 0.2 M H_2SO_4 solution (4.5 mL) and 0.20% DPC solution (0.1 mL) to generate coloured solutions for UV-visible spectra measurement. In general, the reaction was terminated upon achieving a visually colourless state for the Cr(VI)/DPC/H_2SO_4 solution. The solid catalyst after every run was then filtered and successively washed with 1 M HCl, 1M NaOH, deionized water, DMF, and EtOH. The recycled TP-OMS1 was dried under 80 °C and then was used in the subsequent reaction.

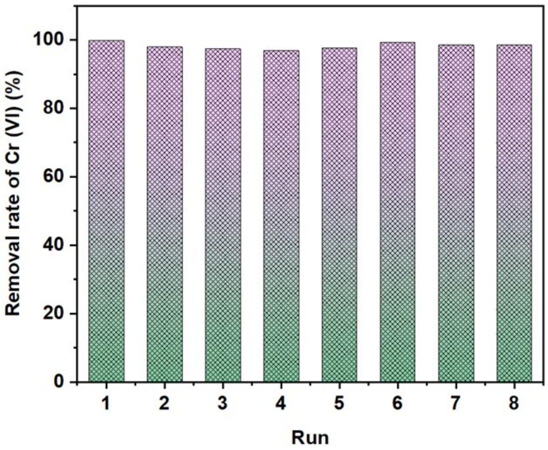

Figure S17. Evaluation for the recyclability of TP-OMS1. All the recycling experiments were performed under the identical conditions as described above.

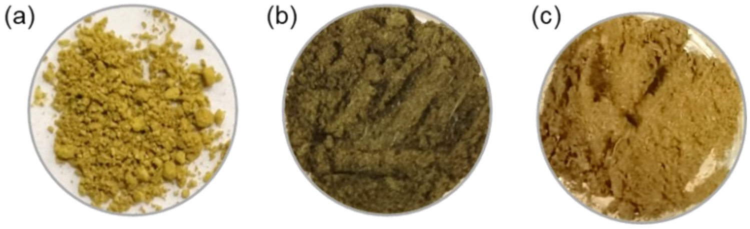

Figure S18. Photographs of fresh TP-OMS1 (a) and the recycled catalyst before (b) and after (c) being washed with 1M HCl and 1M NaOH, successively.

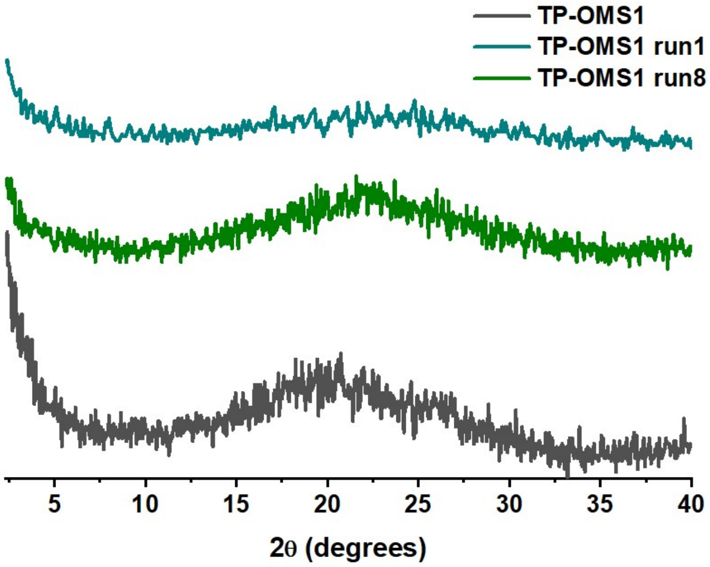

Figure S19. PXRD curves of fresh TP-OMS1 (gray), and the recycled material after the 1st run (dark cyan) and 8 runs (olive).

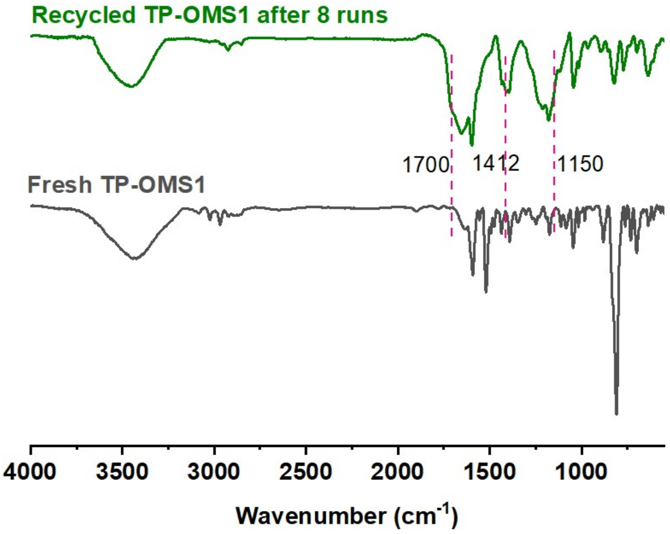

Figure S20. FT-IR spectra of fresh and the recycled TP-OMS1.

The FT-IR spectrum (Figure S22) of the recycled TP-OMS1 after 8 runs reveals that the primary framework of TP-OMS1 remains largely intact. However, distinct new signals are observed, such as carboxyl groups (C=O and C-O) at 1700 cm^{-1} and 1412 cm^{-1}, along with the presence of sulphone (-SO_2-) indicated by the peak at 1150 cm^{-1}. These findings suggest that localized material changes were induced by the strong oxidizing environment.

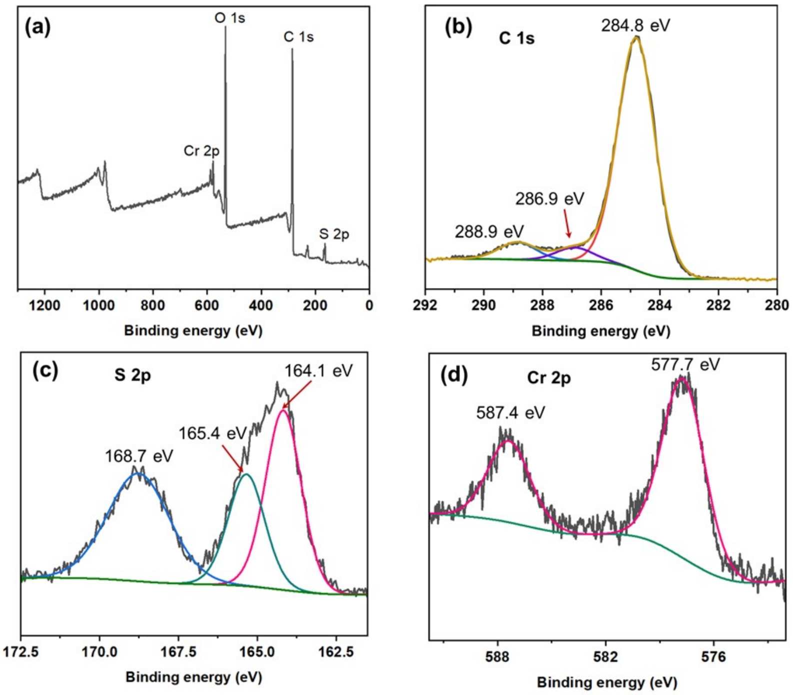

Figure S21. The survey XPS of TP-OMS1 (a); and high-resolution spectra of C 1s (b), S 2p (c) and Cr 2p for residual Cr(III) on the surface of TP-OMS1.

According to Cr 2p peak positions in Figure S23a and S23d, the deconvolution of Cr $2p_{1/2}$ (587. 4 eV) and Cr $2p_{3/2}$ (577.7 eV) can be assigned to Cr(III), which confirmed the reduction of Cr(VI) to Cr(III).[13] The C-S-C bonding from TP unit, *i.e.,* S $2p_{3/2}$ (*ab.* 164.1 eV) and S $2p_{1/2}$ (165.4 eV), which derived from the spin split sulfur coupling could still be observed (Figure S23c).[14-17] The higher binding energy contribution (168.7 eV) observed in TP-OMS1 suggests the presence of sulphone,[14, 18-19] which may arise from TP oxidation by reactive oxygen species (ROS) during photocatalysis. Accordingly, the XPS survey of TP-OMS1 also revealed the presence of O 1s signals, potentially originating from $Cr(OH)_3/Cr_2O_3$, sulphone species, or adsorbed water. Additionally, after 8 catalytic runs, some carbon rings may be oxidized to form carbonyl groups, as indicated by the convolution signal (288.6 eV)[20] observed in the C1s spectrum (Figure S23b). But the signals at 284.5 eV (sp^2 C-C) and 285.1 eV (C-S) demonstrate that the primary framework of TP-OMS1 remains well.[21]

As depicted in Figure S19, the TP-OMS1 exhibited consistent catalytic activity even after 8 successive runs, albeit with a slight increase in reaction time as recycling duration extended. Notably, the N_2 desorption tests (Figure S24) conducted for the recycled catalyst revealed that the BET surface area of TP-OMS1 might play a pivotal role in achieving exceptional catalytic effects. The decrease in OMS pore properties may be due to the gradual deposition of trivalent chromium species ($Cr(OH)_3$, or Cr_2O_3). Additionally, Cr(VI) and ROS generated during the photoreduction may have caused changes of local structure in TP-OMS1 through oxidation, which could also contribute to a deterioration in pore properties.

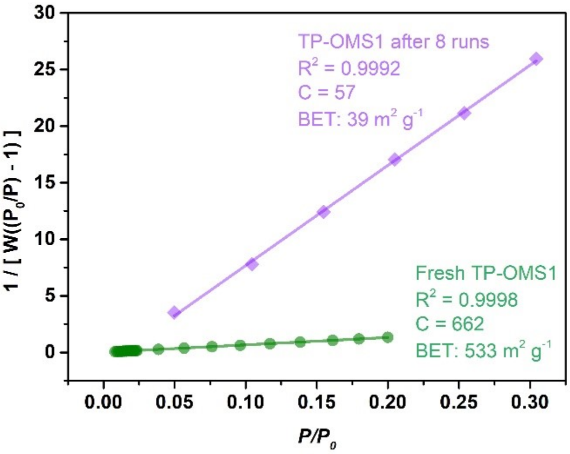

Figure S22. BET surface areas plot of fresh TP-OMS1 (533 m^2 g^{-1}) and the recycled catalyst after the 8th run (39 m^2 g^{-1}).

VI. Mechanism Study

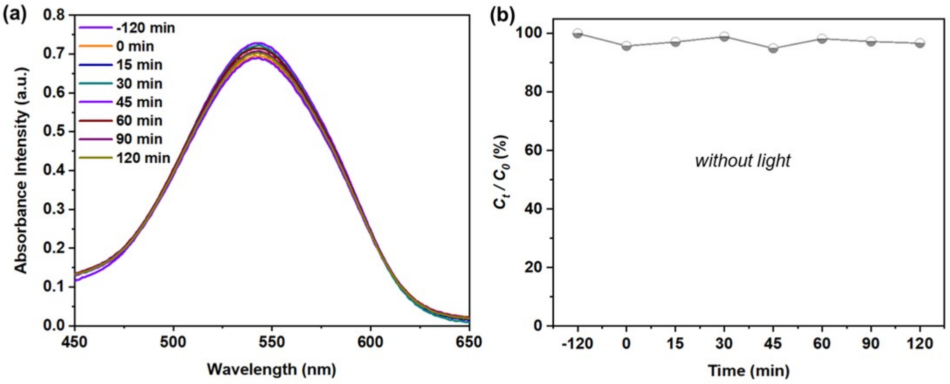

Figure S23. Time-dependent absorbance (a) and concentration (b) changes of Cr(VI) with TP-OMS1 catalyst but no light.

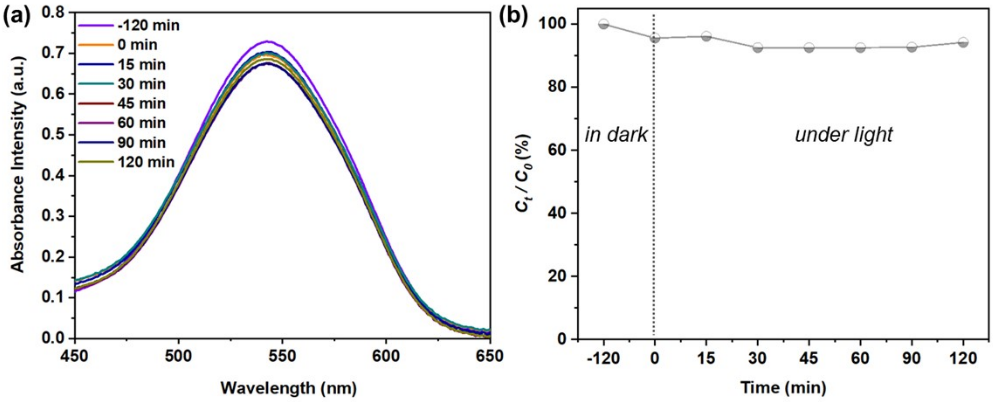

Figure S24. Time-dependent absorbance (a) and concentration (b) changes of Cr(VI) without TP-OMS1 catalyst but using same light irradiation conditions.

For Figure S15 and S16, C_t is the concentration of Cr(VI) after irradiation for different time and C_0 is the initial concentration. The collected Cr(VI) solutions were treated with H_2SO_4 and DPC solution to form colored solutions for UV-visible spectra measurement.

- **Influence of Pd species on the photocatalytic activity:**

(1) Synthetic Procedures for TP-OMS1/Pd[22]

TP-OMS1/Pd-A: $Pd(OAc)_2$ solution in acetone (1.56 mM, 1.35 mL, 2.1 μmol) was added into the mixtures of TP-OMS1 (5 mg) in 0.45 mL H_2O. The system was stirred at 90 ^{o}C for 1 h. The fine powder could be obtained after removing the solvent.

TP-OMS1/Pd-B: $Pd(PPh_3)_4$ (2.43 mg, 2.1 µmol) and TP-OMS1 (5 mg) were combined in 2 mL of CH_2Cl_2, and the mixtures were stirred at 45 °C under a nitrogen atmosphere for 2 hours. The solvent was subsequently removed to yield TP-OMS1/Pd-B.

(2) Photocatalytic performance of TP-OMS1/Pd for Cr(VI) reduction

All the obtained TP-OMS1/Pd-A/B above was directly used for the reduction of Cr(VI). Other *procedures* were conducted according the standard conditions. However, the specially prepared TP-OMS1/Pd-A/B which have higher residual Pd contents, showed slightly inferior performances than the as-synthesized TP-OMS1 (Pd: 0.148 wt%). The results (Figure S19) indicated that the active center of TP-OMSs did not originate from the residual Pd.

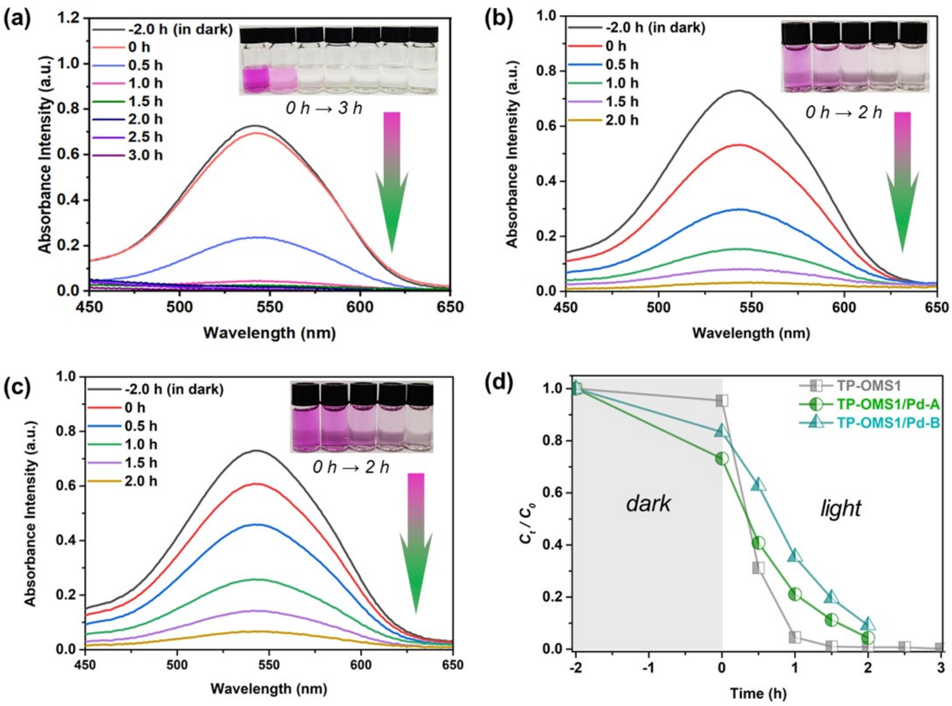

Figure S25. Time-dependent absorbance and color changes of Cr(VI) derived by (a)TP-OMS1, (b) TP-OMS1/Pd-A, or (c)TP-OMS1/Pd-B. (d) Time-dependent concentration changes of Cr(VI) mediated by TP-

OMS1 or TP-OMS1/Pd. *The collected Cr(VI) solutions were treated with H_2SO_4 and DPC solution to form colored solutions for UV-visible spectra measurement.*

- ***•OH radicals detection test:***

5 mg of TP-OMSs was dispersed in an 8 mL aqueous solution containing 10 mM NaOH and 5 mM terephthalic acid (TA). Then, 0.32 mL of acetone was added to the reaction system. The suspension was stirred in the dark for 0.5 h before being subjected to visible light irradiation. After irradiated under visible light for 0.5 h, the mixture was filtered through a 0.22 μm filter to remove the photocatalysts for fluorescence spectroscopy measurements. The fluorescence of the in-situ produced 2-hydroxy-terephthalic acid (TAOH) was measured using a fluorescence spectrophotometer with an excitation wavelength of 320 nm.

$$\text{TP-OMS1} \xrightarrow{hv} \text{TP-OMS1 }(e^-) + \text{TP-OMS1 }(h^+) \tag{Eq. S1}$$

$$CrO_4^{2-} + 3\text{TP-OMS1 }(e^-) + 4H_2O \longrightarrow Cr(OH)_3 + 5OH^- + \text{TP-OMS1} \tag{Eq S2}$$

$$O_2 + \text{TP-OMS1 }(e^-) \longrightarrow O_2^{\bullet-} + \text{TP-OMS1} \tag{Eq. S3}$$

$$CrO_4^{2-} + O_2^{\bullet-} + 3H_2O \longrightarrow Cr(OH)_3 + 3OH^- + 1.5\,O_2 \tag{Eq. S4}$$

$$O_2^{\bullet-} + H^+ \longrightarrow {}^{\bullet}OOH \xrightarrow{\text{TP-OMS1 }(e^-) + H^+} H_2O_2 + \text{TP-OMS1} \tag{Eq. S5}$$

$$0.5O_2 + H_2O \xrightarrow{2\text{TP-OMS1 }(e^-)} H_2O_2 + \text{TP-OMS1} \tag{Eq. S6}$$

$$H_2O_2 + \text{TP-OMS1 }(e^-) \longrightarrow OH^- + {}^{\bullet}OH + \text{TP-OMS1} \tag{Eq. S7}$$

$$2{}^{\bullet}OH \longrightarrow 0.5O_2 + H_2O \tag{Eq. S8}$$

$$2{}^{\bullet}OH \longrightarrow H_2O_2 \tag{Eq. S9}$$

$$H_2O + \text{TP-OMS1 }(h^+) \longrightarrow 0.5O_2 + 2H^+ + \text{TP-OMS1} \tag{Eq. S10}$$

Scheme S4. Mechanism demonstrations for TP-OMSs mediated photoreduction of Cr(VI) through reaction equations.

Table S2. Electrode potential or energy levels (*vs.* NHE) for TP-OMSs, ROS and Cr(VI)/Cr(III) redox couples. [23-28]

E(Cr(VI)/Cr(III))	*vs.* NHE	+ 0.51 V
$E(O_2/O_2^{\bullet-})$		+ 0.33 V
$E(O_2/H_2O)$		+ 1.23 V
$E(H_2O_2/OH^-)$		+ 0.73 V
$E({}^{\bullet}OH_2/H_2O_2/H^+)$		+ 1.44 V
$E(O_2/H_2O_2)$		+0.68 V
$E({}^{\bullet}OH/H_2O)$		+ 2.73 V
$E({}^{\bullet}OH/OH^-)$		+ 1.99 V
E^c(TP-OMS1)		- 0.76 V
E^v(TP-OMS1)		+ 1.84 V
E^c(TP-OMS2)		- 0.90 V
E^v(TP-OMS2)		+ 1.42 V

VII. Catalytic Comparison with Some Reported Photocatalysts

Table S3. Representative heterogeneous catalysts for the photoreduction of Cr(VI)

Type	**Catalyst**	**Concentration of Cr(VI)**	**Irradiation time (min)**	**hole scavenger agents**	**pH value**	**degradation degree**	**Ref.**
Polymer	TPB-BT-COF	10 mg/L	75	no	7	99%	*J. Mater. Chem. A*, **2019**, *7*, 998–1004
	TAPT-BT-COF	10 mg/L	105	no	7	99%	
	TPB-TP-COF	10 mg/L	105	no	7	80%	
	TAPP-2F	5 mg/L	120	no	3	Nearly 100%	*J. Hazard. Mater.*, **2024**, *476*, 134956
	COF-PDZ	5 mg/L	20	no	7	95%	*Environ. Sci. Technol.* 2021, 55, 5371−5381
	Tp-Tta-COOH,	50 mg/L	120	no	1	99%	*Appl. Catal. B: Environ. and Energy* 344 (2024) 123672
	g-C_3N_4	10 mg/L	180	no	3	50%	*Appl. Surf. Sci.,* **2017**, *425*, 107.
	HDU-26	10 mg/L	60	no	3	99.5	*Environ. Sci.: Nano*, **2024**, *11*, 229–240
	PYE-COF	10 mg/L	60	no	7	100%	*Mater. Chem. Front.*, **2022**, *6*, 3748–3754
	Py-SO_1	10 mg/L	90	no	4	93%	*J. Hazard. Mater.* **2022**, *434*, 128938.
	TACTF@CNT	50 mg/L	120	BA	7	100%	*J. Environ. Chem. Eng.,* **2023** *11*, 109331.
	TP-OMS1	10 mg/L	90 (120)	no	7	99% (Nearly 100%)	This work
	TP-OMS1	100 mg/L	240	no	7	Nearly 100%	
	TP-OMS2	10 mg/L	120 (150)	no	7	94% (>99%)	
MOF	NNU-36	10 mg/L	60	CH_3OH	2.17	95.3%	*ACS Sustainable Chem. Eng.* **2017**, *5*, 4449−4456
	MIL-68(In)–NH_2	20 mg/L	180	EtOH	2	97%	*Appl. Catal., B,* **2015**, *162*, 245–251
Inorganic Materials	TiO_2	20 mg/L	60	no	7	80%	*RSC Adv.*, **2017**, *7*, 8004.
	MCRCSs	30 mg/L	120	no	2	100%	*New J. Chem.*, **2017**, *41*, 12596-12603
	$BiVO_4/Bi_2S_3$ (H-3)	10 mg/L	60	no	7	91.2%	*Angew. Chem. Int. Ed.*, **2014**, *53*, 5917.

VIII. References

[1] W.-H. Huang, W.-L. Jia, S. Wang, *Can. J. Chem.* **2006**, *84*, 477-485.

[2] W.-K. An, S.-J. Zheng, Y.-N. Du, S.-Y. Ding, Z.-J. Li, S. Jiang, Y. Qin, X. Liu, P.-F. Wei, Z.-Q. Cao, M. Song, Z. Pan, *Catal. Sci. Technol.* **2020**, *10*, 5171-5180.

[3] M. Dogru, M. Handloser, F. Auras, T. Kunz, D. Medina, A. Hartschuh, P. Knochel, T. Bein, *Angew. Chem. Int. Ed.* **2013**, *52*, 2920-2924.

[4] R. Z. Lange, G. Hofer, T. Weber, A. D. Schlüter, *J. Am. Chem. Soc.* **2017**, *139*, 2053-2059.

[5] J.-X. Jiang, F. Su, A. Trewin, C. D. Wood, N. L. Campbell, H. Niu, C. Dickinson, A. Y. Ganin, M. J. Rosseinsky, Y. Z. Khimyak, A. I. Cooper, *Angew. Chem. Int. Ed.* **2007**, *46*, 8574-8578.

[6] N. Ritter, I. Senkovska, S. Kaskel, J. Weber, *Macromol. Rapid Commun.* **2011**, *32*, 438-443.

[7] Y. Lan, C. Yang, Y. Zhang, W. An, H. Xue, S. Ding, P. Zhou, W. Wang, *Polym. Chem.* **2019**, *10*, 3298-3305.

[8] W.-K. An, M.-Y. Han, C.-A. Wang, S.-M. Yu, Y. Zhang, S. Bai, W. Wang, *Chem. Eur. J.* **2014**, *20*, 11019-11028.

[9] C. Ayed, L. Caire da Silva, D. Wang, K. A. I. Zhang, *J. Mater. Chem. A* **2018**, *6*, 22145-22151.

[10] S. Grätz, M. Oltermann, E. Troschke, S. Paasch, S. Krause, E. Brunner, L. Borchardt, *J. Mater. Chem. A* **2018**, *6*, 21901-21905.

[11] M. G. Kotp, N. L. Torad, H. Nara, W. Chaikittisilp, J. You, Y. Yamauchi, A. F. M. El-Mahdy, S.-W. Kuo, *J. Mater. Chem. A* **2023**, *11*, 15022-15032.

[12] Z. Yan, Y. Luo, B. Chen, F. Wang, L. Chen, Z. Wang, P. Zhao, J. Kang, Z. Fu, Y. Jin, Y. Wang, C. Xia, *Chem. Eng. J.* **2023**, *453*, 139934.

[13] F. Liu, Z. Ma, Y. Deng, M. Wang, P. Zhou, W. Liu, S. Guo, M. Tong, D. Ma, *Environ. Sci. Technol.* **2021**, *55*, 5371-5381.

[14] W.-K. An, X. Xu, S.-J. Zheng, Y.-N. Du, J. Ouyang, L.-X. Xie, Y.-L. Ren, M. He, C.-L. Fan, Z. Pan, Y.-H. Li, *ACS Catal.* **2023**, *13*, 9845-9856.

[15] D. C. Martin, J. Wu, C. M. Shaw, Z. King, S. A. Spanninga, S. Richardson-Burns, J. Hendricks, J. Yang, *Polym. Rev.* **2010**, *50*, 340-384.

[16] W. Du, Y. Qin, C. Ni, W. Dai, J. Zou, *ACS Appl. Polym. Mater.* **2020**, *2*, 5121-5128.

[17] L. Guo, Y. Niu, H. Xu, Q. Li, S. Razzaque, Q. Huang, S. Jin, B. Tan, *J. Mater. Chem. A* **2018**, *6*, 19775-19781.

[18] Q. Ma, J. Zheng, H. Kang, L. Zhang, Q. Zhang, H. Li, R. Wang, T. Zhou, Q. Chen, A. Liu, H. Li, C. Zhang, *ACS Appl. Mater. Interfaces* **2021**, *13*, 43002-43010.

[19] B. An, Q.-h. Zhang, B.-s. Zheng, M. Li, Y.-y. Xi, X. Jin, S. Xue, Z.-t. Li, M.-b. Wu, W.-t. Wu, *Angew. Chem. Int. Ed.* **2022**, *61*, e202204661.

[20] S. Zhao, K. Yang, L. Jiang, J. Xiao, B. Wang, L. Zeng, X. Song, M. Lan, *ACS Appl. Nano Mater.* **2021**, *4*, 10528-10533.

[21] J. Li, F. Zhao, F. Nan, J. Wang, Y. Zhang, K. Liang, X. Xue, T. Chen, L. Kong, J. Ge, P. Wang, *Chin. J. Chem.* **2023**, *41*, 1950-1956.

[22] Z. J. Wang, S. Ghasimi, K. Landfester, K. A. I. Zhang, *Chem. Mater.* **2015**, *27*, 1921-1924.

[23] W. Lu, C. Wang, Y. Bai, C. Xie, Z. Zhang, W. Song, J. Wang, *Environ. Sci.: Nano* **2024**, *11*, 229-240.

[24] X. Zhang, F. Tian, L. Qiu, M. Gao, W. Yang, Y. Liu, Y. Yu, *J. Mater. Chem. A* **2021**, *9*, 10297-10303.

[25] M. Hussain, A. Saddique, K. C. Devarayapalli, B. Kim, I. W. Cheong, D. S. Lee, *Appl. Catal. B: Environ. Energy* **2024**, *344*, 123672.

[26] A. Chen, Z. Jiang, J. Tang, G. Yu, *Prog. Chem.* **2024**, *36*, 357-366.

[27] Q. Zhi, W. Liu, R. Jiang, X. Zhan, Y. Jin, X. Chen, X. Yang, K. Wang, W. Cao, D. Qi, J. Jiang, *J. Am. Chem. Soc.* **2022**, *144*, 21328-21336.

[28] W. Lu, C. Wang, W. Song, Z. Zhang, C. Xie, J. Wang, *J. Mater. Chem. A* **2024**, *12*, 20149-20159.

IX. Liquid NMR Spectra of Some Compounds

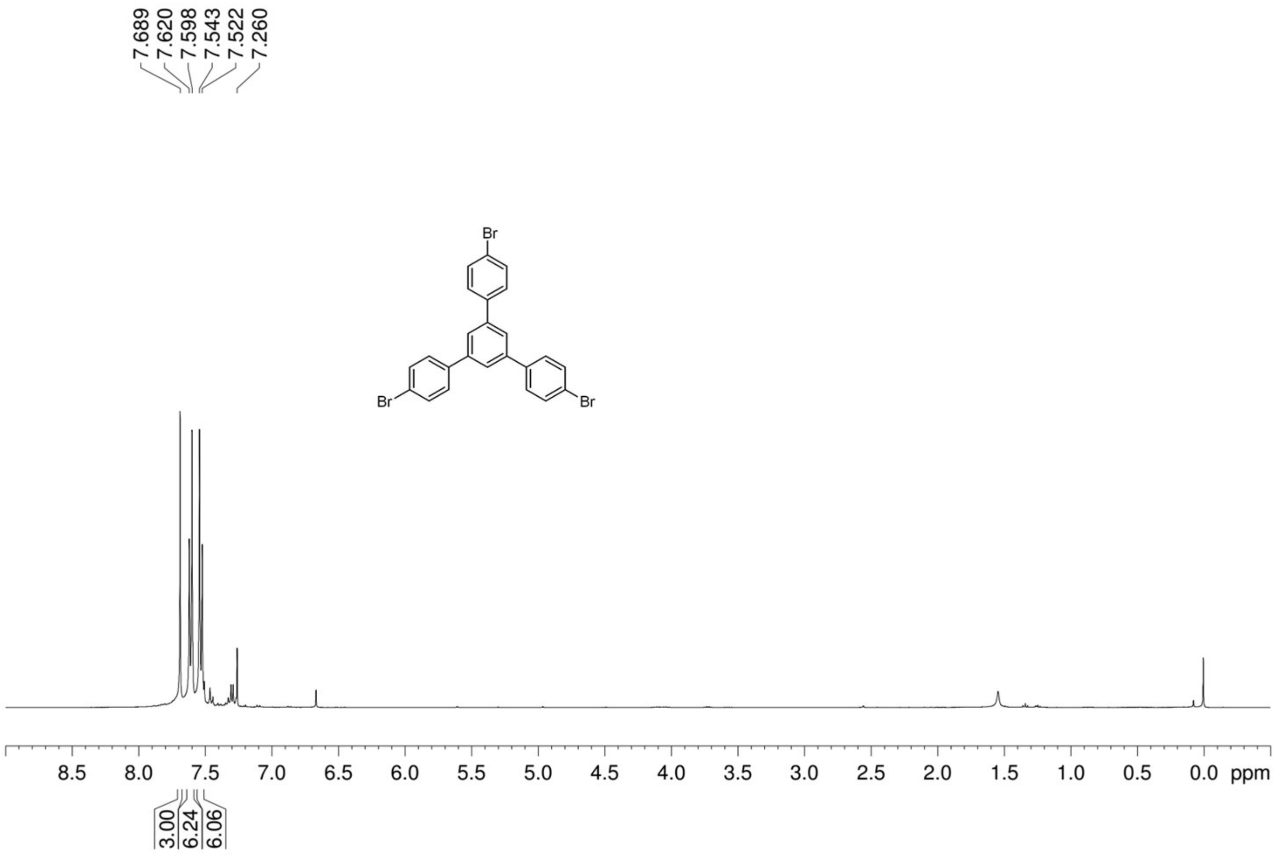

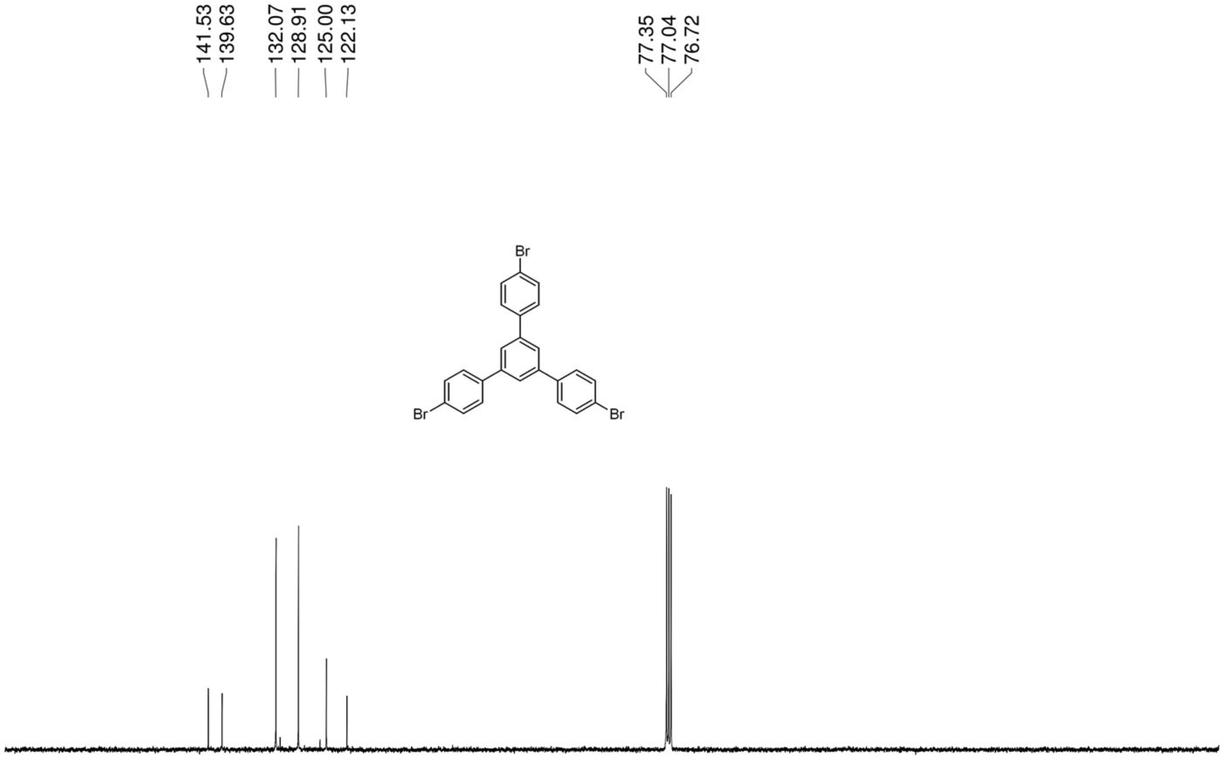

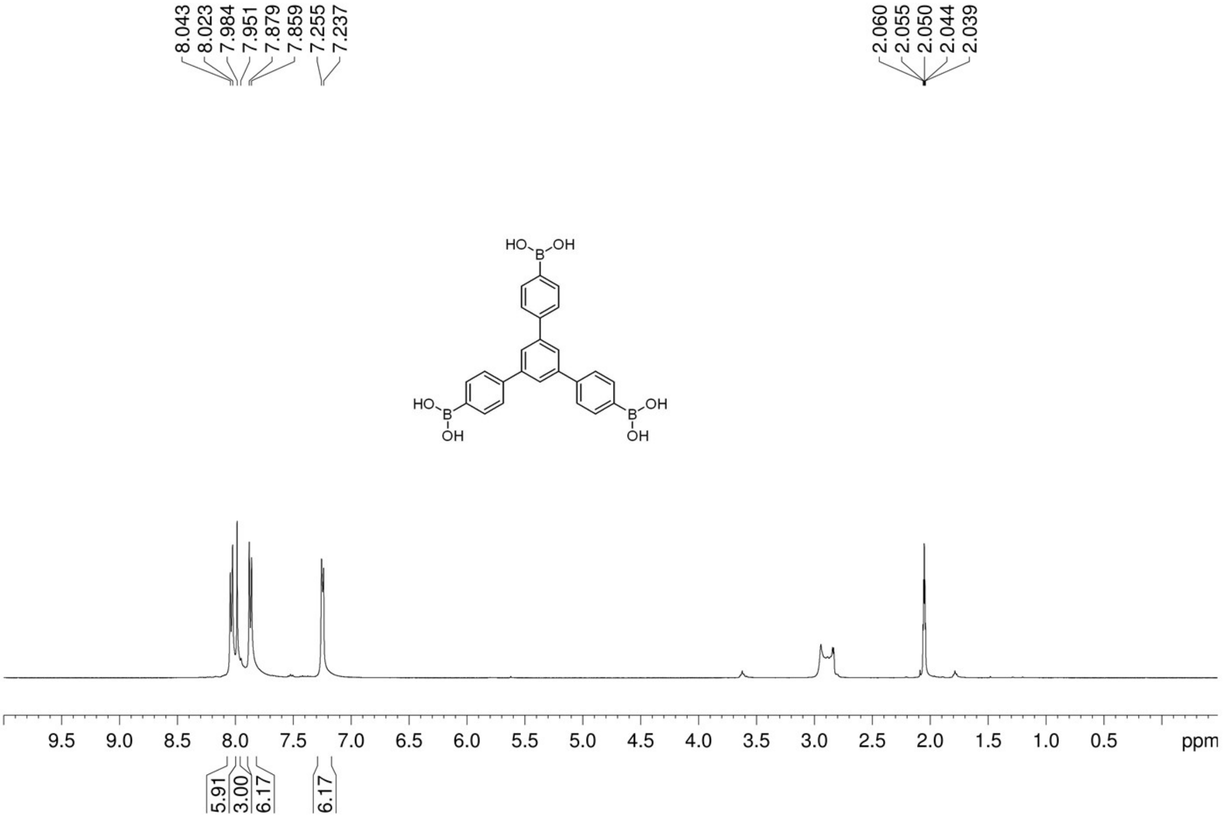
8.043
8.023
7.984
7.951
7.879
7.859
7.255
7.237
2.060
2.055
2.050
2.044
2.039
HO
B
OH
9.5
9.0
8.5
8.0
7.5
7.0
6.5
6.0
5.5
5.0
4.5
4.0
3.5
3.0
2.5
2.0
1.5
1.0
0.5
ppm
5.91
3.00
6.17
6.17

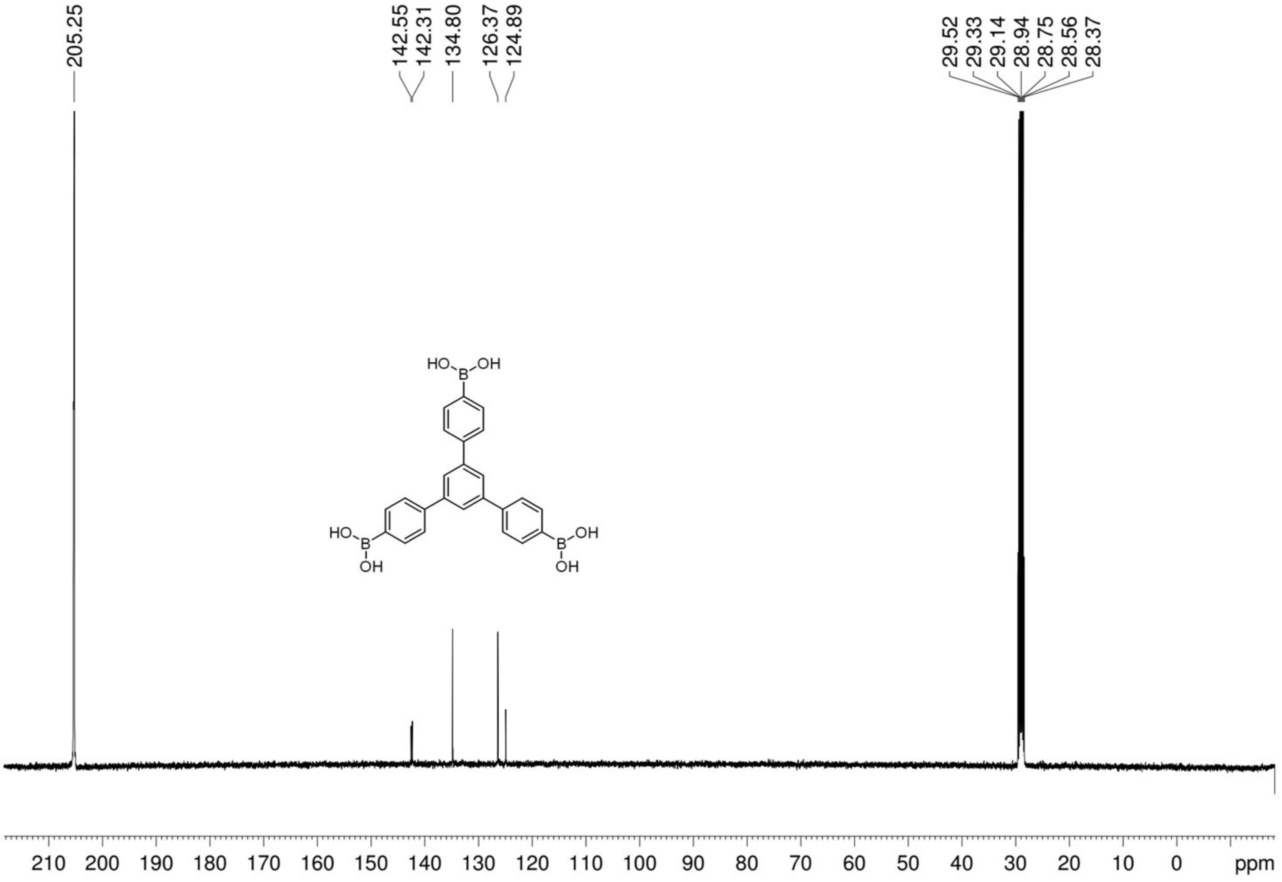
205.25
142.55
142.31
134.80
126.37
124.89
29.52
29.33
29.14
28.94
28.75
28.56
28.37
HO
B
OH
210
200
190
180
170
160
150
140
130
120
110
100
90
80
70
60
50
40
30
20
10
0
ppm

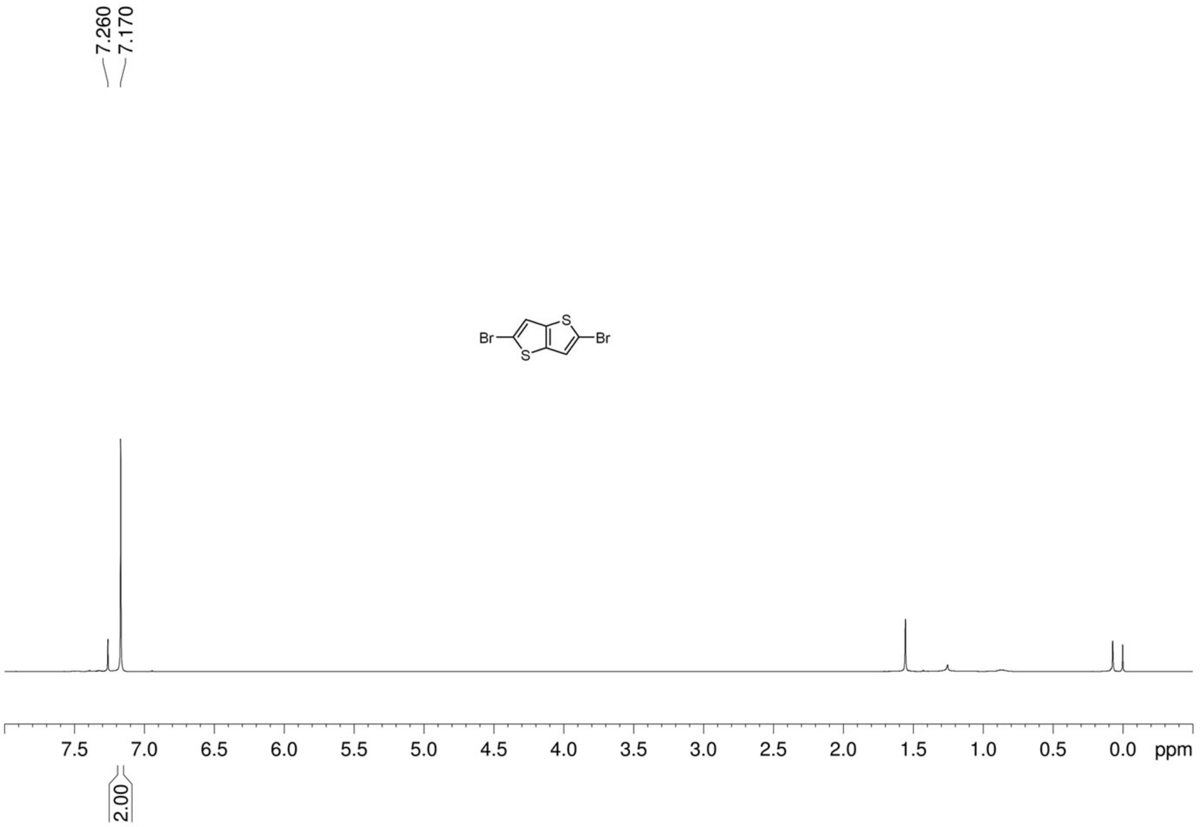
7.260
7.170
Br
S
S
Br
7.5
7.0
6.5
6.0
5.5
5.0
4.5
4.0
3.5
3.0
2.5
2.0
1.5
1.0
0.5
0.0
ppm
2.00

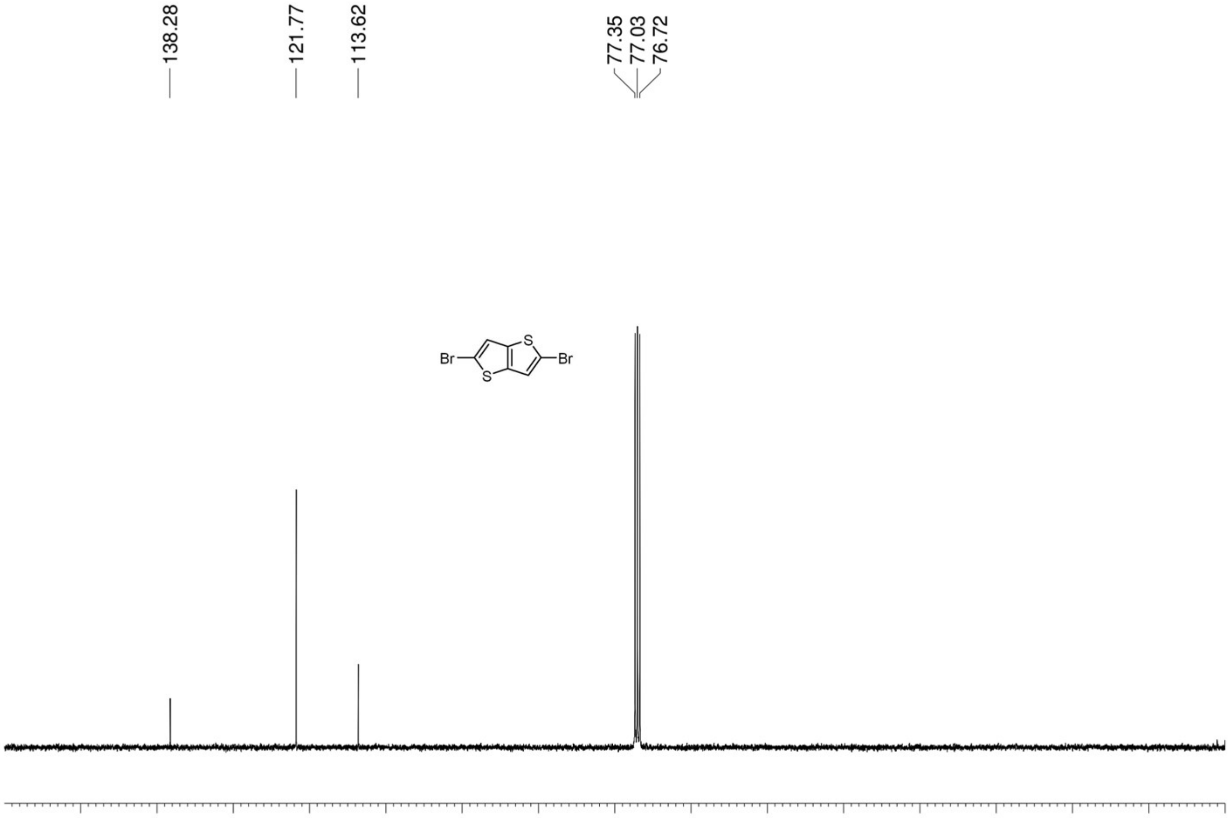
138.28
121.77
113.62
77.35
77.03
76.72
Br
S
S
Br
150
140
130
120
110
100
90
80
70
60
50
40
30
20
10
ppm